Journal of Power Sources 216 (2012) 76–83

Contents lists available at SciVerse ScienceDirect

Journal of Power Sources

journal homepage: www.elsevier.com/locate/jpowsour

High-capacity cathodes for lithium-ion batteries from nanostructured $LiFePO_4$ synthesized by highly-flexible and scalable flame spray pyrolysis

N.A. Hamid [a], S. Wennig [b], S. Hardt [a], A. Heinzel [b], C. Schulz [a,c], H. Wiggers [a,c,*]

[a] Institute for Combustion and Gasdynamics (IVG), University of Duisburg-Essen, Duisburg, Germany
[b] Centre for Fuel Cell Technology, ZBT Duisburg, Germany
[c] CENIDE Center for Nanointegration, Duisburg-Essen, Germany

HIGHLIGHTS

- Nanosized $FePO_4 \cdot xH_2O$ was synthesized using highly scalable flame spray pyrolysis.
- High purity Nano-$LiFePO_4$/C composite was produced by a subsequent solid-state reaction.
- Material consists of $LiFePO_4$ NPs homogeneously distributed in a carbon matrix.
- Material has a good discharge capacity of more than 140 mAh g^{-1}.
- Very high drain rates of 16 C while delivering 40 mAh g^{-1} are shown without degradation.

ARTICLE INFO

Article history:
Received 16 March 2012
Received in revised form
2 May 2012
Accepted 16 May 2012
Available online 24 May 2012

Keywords:
Flame spray pyrolysis
Nanoscale $FePO_4$
Specific surface area
$LiFePO_4$/C composite
Electrochemical properties

ABSTRACT

Olivine, $LiFePO_4$ is a promising cathode material for lithium-ion batteries due to its low cost, environmental acceptability and high stability. Its low electric conductivity prevented it for a long time from being used in large-scale applications. Decreasing its particle size along with carbon coating significantly improves electronic conductivity and lithium diffusion. With respect to the controlled formation of very small particles with large specific surface, gas-phase synthesis opens an economic and flexible route towards high-quality battery materials. Amorphous $FePO_4$ was synthesized as precursor material for $LiFePO_4$ by flame spray pyrolysis of a solution of iron acetylacetonate and tributyl phosphate in toluene. The pristine $FePO_4$ with a specific surface from 126–218 m^2 g^{-1} was post-processed to $LiFePO_4$/C composite material via a solid-state reaction using Li_2CO_3 and glucose. The final olivine $LiFePO_4$/C particles still showed a large specific surface of 24 m^2 g^{-1} and were characterized using X-ray diffraction (XRD), electron microscopy, X-ray photoelectron spectrocopy (XPS) and elemental analysis. Electrochemical investigations of the final $LiFePO_4$/C composites show reversible capacities of more than 145 mAh g^{-1} (about 115 mAh g^{-1} with respect to the total coating mass). The material supports high drain rates at 16 C while delivering 40 mAh g^{-1} and causes excellent cycle stability.

1. Introduction

The increasing utilization of renewable energy as well as the increasing production of electrically driven vehicles requires a significant improvement for electrical energy storage. With respect to performance and storage capacity, rechargeable lithium-ion batteries have become one of the best options for mobile applications such as laptops, consumer electronics, power tools and others since their first commercial introduction in the early 1990s. Safety, increased capacity, power and availability are of increasing importance with respect to the mass application of Li-ion batteries. At the cathode of Li-ion batteries, Li^+ is typically stored in transition metal oxides such as $LiCoO_2$, $LiNiO_2$, and other Ni- or Co-based mixed oxides [1] that considerably contribute to the cost and weight of a battery.

Olivine ($LiFePO_4$) has gained more and more attention as cathode material due to its advantages compared to the commonly used materials. Especially its environmental safety, sustainability, availability and expected low production cost in combination with its theoretical storage capacity of 170 mAh g^{-1} makes it a highly interesting cathode material. Even though having many advantages, the poor electronic conductivity and Li-ion diffusion of

* Corresponding author. University of Duisburg-Essen, Lotharstr. 1, 47057 Duisburg, Germany. Tel.: +49 203 3793156; fax: +49 203 3793087.
E-mail address: hartmut.wiggers@uni-due.de (H. Wiggers).

0378-7753/$ – see front matter © 2012 Elsevier B.V. All rights reserved.
doi:10.1016/j.jpowsour.2012.05.047

conventional $LiFePO_4$ compared to the established materials has prevented it from being used in the battery market. The most promising approach to overcome these problems focus on decreasing the particles size to the nanometer range and coating them with electrically conducting materials [2–13]. Various research groups investigated the utilization of $FePO_4 \cdot xH_2O$ based on cost-efficient raw material to produce high-rate $LiFePO_4$. Several routes such as the polymer–pyrolysis–reduction method [7], the sol–gel route [8,9], the modified co-precipitation method [12,14], the rheological phase method [11,15,16], the carbothermal reduction method [6,17–19], the microwave method [20], the solid-state reaction method [3,21–23], and the solid/liquid phase reaction [24,25] were investigated in search for a promising route suitable for up scaling purposes.

Typically, the performance of $LiFePO_4$/C is determined by the production strategy of the raw material, the electrode preparation, and the amount of carbon used as conducting agent. Recently, Liu et al. [2] used high temperature heat-treatment of 20–50 nm $FePO_4$/polythiophene mixtures to produce $LiFePO_4$/C with improved cycling performance and high initial discharge capacity of 150 mAh g^{-1} at 0.1 C rate (i.e., charging and discharging of 10% of the nominal power). Promising electrochemical performance with an excellent initial discharge capacity of 157 mAh g^{-1} was found at high temperature using the polymer–pyrolysis–reduction method [7]. Peng et al. [8] reported the use of 100–500 nm $LiFePO_4$/C from $FePO_4 \cdot xH_2O$ produced by sol–gel method with a discharge capacity of about 106 mAh g^{-1} at 10 C rate providing a capacity retention of 98.7% after the 50th cycle. Nanosized $LiFePO_4$ ranging from 20–30 nm with a high amount of carbon was successfully produced using the sol–gel method yielding an initial discharge capacity of 126 mAh g^{-1} at 0.1 C [9]. While many groups produce and investigate nanosized $LiFePO_4$/C, Lou et al. describe micrometer-sized $LiFePO_4$/C exhibiting a discharge capacity of 116, 96 and 75 mAh g^{-1} at 10, 20, and 30 C, respectively. Huang et al. [11] produced $FePO_4 \cdot 2H_2O$ by a rheological phase method with sizes between 60 and 150 nm showing high discharge capacity of 160 mAh g^{-1} and 155 mAh g^{-1} at 0.5 C and 1 C, correspondingly. Fine $LiFePO_4$/C with good cycling stability and a capacity of 134 mAh g^{-1} at 2 C was prepared by Wang et al. [12]. Furthermore, $LiFePO_4$/C formed using $FePO_4 \cdot 2H_2O$ via the carbothermal route showed an initial capacity of 133, 151.2, and 144 mAh g^{-1} at 0.1 to 0.2 C [17–19].

Although the nanoscale $LiFePO_4$/C composite materials produced by the above mentioned routes illustrated quite good electrochemical results, in most cases the production process was found to be too complicated for large-scale production. While large amounts of conductive carbon lead to better electrochemical properties, the tap density and energy density are decreased gradually. Therefore, the amount of conductive carbon must be kept to a minimum to optimize the electrochemical performance of the cathode material. In addition, the cost of the raw material, especially the source for the iron compound, must be considered with respect to mass production. Additionally, in most of the previous works the production of large specific surface $FePO_4 \cdot xH_2O$ or $LiFePO_4$/C was not possible. We investigated a method based on flame spray pyrolysis (FSP) which is known to enable the production of significant amounts of nanosized materials with the potential to be scaled to industrial production scales. First approaches towards $LiFePO_4$/C produced by FSP have been made before [26], but the results revealed that for good performance and sufficiently reducing conditions during synthesis, a large amount of carbon is produced as a secondary product, which unfortunately lowers the overall capacity significantly. Nevertheless, FSP is a particularly suitable and scalable method to synthesize nanomaterials from cheap raw material of iron (III) such as iron nitrate or iron chloride. Therefore, we developed a two-step method towards the formation of nanoscale $LiFePO_4$/C composite materials. For simplicity reasons and to avoid the formation of nitrogen oxides and hydrochloric acid, we synthesized large specific surface $FePO_4 \cdot xH_2O$ from iron (III) acetylacetonate while the final nanoscale high-performance $LiFePO_4$/C is generated from a mixture of $FePO_4 \cdot xH_2O$, Li_2CO_3, and glucose. The results presented here demonstrate the viability of the synthesis strategy as well as the good cycling stability and electrochemical properties of the product.

2. Experimental

2.1. Powder synthesis

The basic raw material $FePO_4 \cdot xH_2O$ was prepared in the gas-phase using the flame spray pyrolysis technique known from literature [27]. Three different liquid precursor solutions consisting of iron (III) acetylacetonate and tri-butylphosphate (reagent grade, Merck) in toluene (reagent grade, Merck) were prepared with iron and phosphate concentrations of 0.0125, 0.05, and 0.2 mol l^{-1}, respectively. At a constant flow rate of 3 ml min^{-1}, the precursor solutions were injected into a flame spray pyrolysis reactor via a water-cooled air-blast nozzle using a feeding system consisting of two syringe pumps for continuous operation. A coaxial dispersion gas flow of 5 slm O_2 (Air Liquide, purity 99.95%) was used for the atomization of the liquid precursor solution. The resulting spray was ignited and the highly-turbulent spray flame was stabilized by a supporting premixed methane/oxygen flame at a flow rate of 2.4 slm O_2 and 1.13 slm CH_4 (Air Liquide, purity 99.95%). An additional sheath gas flow of 5 slm O_2 was fed through a sinter metal ring with an inner diameter of 18 mm and an outer diameter of 34 mm surrounding the supporting flame to ensure complete conversion of the reactants and to stabilize the fluid flow. The gas flows were adjusted by mass flow controllers (Bronkhorst). The flame is located in a 330 mm diameter stainless-steel housing and the product was collected from the exhaust gas on a filter located downstream of the flame spray reactor. Fig. 1 shows a sketch of the flame spray reactor used in this work.

The $LiFePO_4$/C composite material was synthesized via a solid-state reaction from a mixture of the as-prepared $FePO_4$, Li_2CO_3 (reagent grade, Merck), and glucose as reducing agent and carbon source. After pre-heating, the intimately mixed powder was pelletized and calcinated for 16 h at 600 °C under inert gas atmosphere. A black-colored product with a tap density of 1.42 g cm^2 was obtained after cooling down to room temperature.

2.2. Material characterization

The phase composition of all products was determined by X-ray diffraction (XRD) performed with a PANalytical X-ray diffractometer (X'Pert PRO) with Cu K_α-radiation (1.5406 Å). From the XRD pattern the crystallite size was calculated by Rietveld refinement using the program MAUD [28]. The specific surface area was determined by nitrogen adsorption using the Brunauer–Emmet–Teller method (BET, Quantachrome Nova2000). Thermogravimetric analysis was conducted using a commercial TGA/DTA instrument (Bähr STA 503). The morphology of the materials was investigated by transmission electron microscopy (TEM, Philips CM12) with an accelerating voltage of 120 kV. The carbon content of the $LiFePO_4$/C composite was determined by an element analyzer (CE instruments EA1110) and X-ray photoelectron spectroscopy (XPS, SPECS Phoibos 100) was performed to determine the oxidation state of iron in $LiFePO_4$/C. Raman spectroscopy was performed with a micro-Raman system using a wavelength of 532 nm and a liquid-nitrogen cooled CCD for

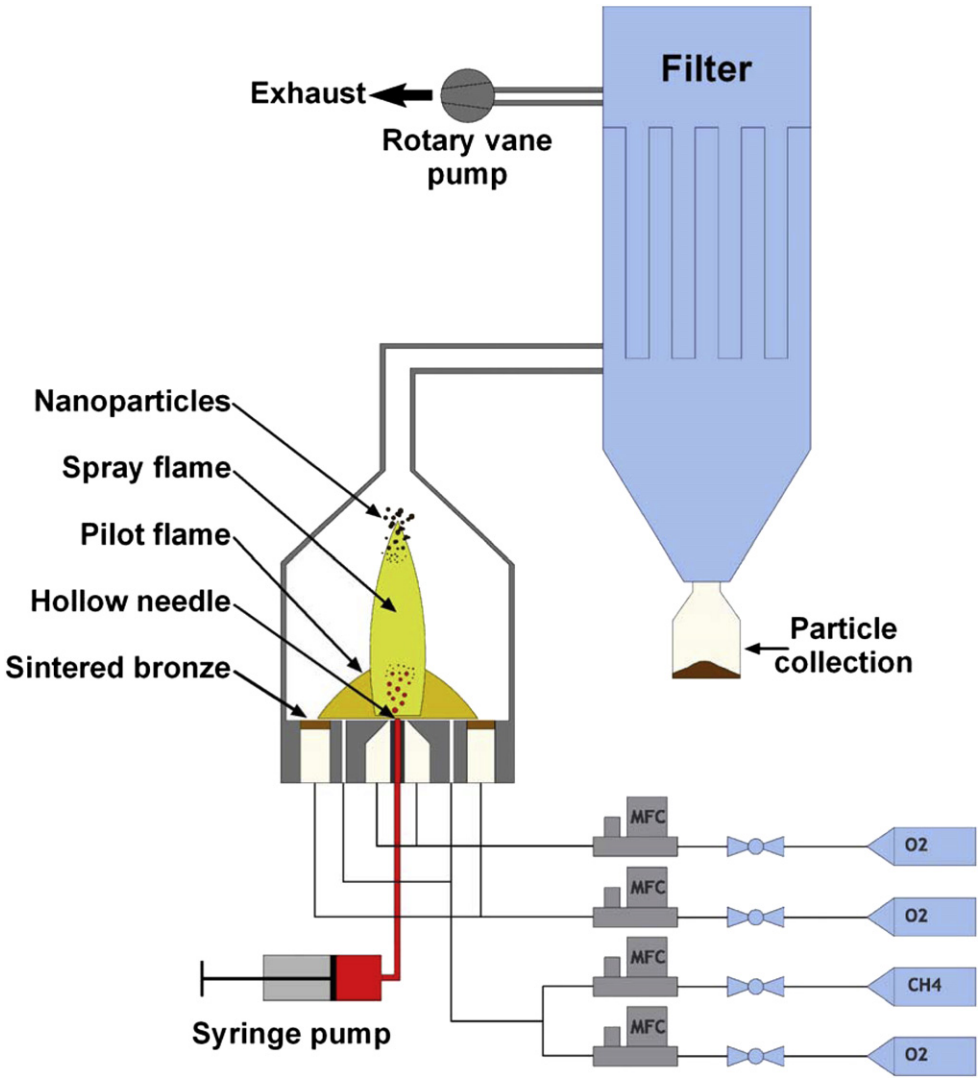

Fig. 1. Schematic representation of the experiment used for flame spray pyrolysis.

detection. The spot size of the laser beam on the sample surface was focused with a microscope lens to about 1 μm diameter and the spectra were recorded at room temperature in backscattering geometry.

2.3. Electrode preparation

$LiFePO_4$/C and Super-P Li™ (Timcal) were intensely mixed in a mortar and subsequently dispersed in *N*-methyl-*2*-pyrrolidone (NMP, Acros Organics, extra dry, water < 50 ppm) together with polyvinylidene fluoride (PVdF, Solef 1013, Solvay Solexis). After sonication, the dispersions were either homogenized by means of a turbo mixer at 10,000 rpm for 60 min or by further sonication. We found that the decreased tap density didn't have any influence on the preparation of the dispersion in comparison to commercially available $LiFePO_4$ materials with higher tap density. The obtained slurry was cast on an aluminum foil (Alujet, thickness: 30 μm) with a wet film thickness of 150 μm by using an adjustable doctor blade and dried under vacuum at 120 °C. Afterwards, the samples were compressed by calendaring and cut into electrodes with an area of 1.1 cm^2. The typical composition of the dried electrodes was 86 wt% $LiFePO_4$/C, 7 wt% Super-P Li™ and 7 wt% PVdF. The average mass loading of the electrodes was around 4.0 mg cm^{-2}.

2.4. Electrochemical tests

Electrochemical measurements were carried out using Swagelok(R)-type electrode cells. Lithium foil (Chemetall, 100 μm thick) served as counter and reference electrodes and polypropylene fleeces impregnated with electrolyte were used as separator. As electrolyte a solution of 1 M $LiPF_6$ in ethylene carbonate and diethyl carbonate (3/7; *m*/*m*) was used. The test cells were assembled in an argon filled glove box.

Constant current (CC) tests and cyclic voltammetry (CV) measurements were performed with a Basytec CTS Lab XL battery tester. CC experiments were carried out in the range of 2.4 to 4.0 V vs. Li/Li^+ and CV measurements were recorded between 2.3 and 4.0 V vs. Li/Li^+ with a scan rate of 10 μV s^{-1}. Impedance spectra were recorded with an electrochemical workstation (Zahner IM6) at a potential of 3.0 V vs. Li/Li^+ in a frequency range between 10 mHz and 3 MHz at an amplitude of 5 mV.

3. Results and discussion

X-ray powder diffraction patterns were used to analyze the structure and identify the phase of the as-prepared $FePO_4$ before and after annealing at 600 °C in air (see Fig. 2). While in all cases the

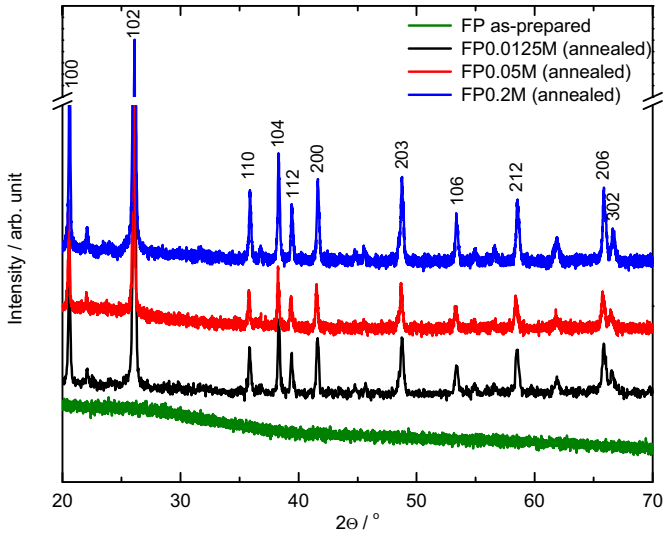

Fig. 2. XRD patterns of as-prepared and thermally-annealed (600 °C) $FePO_4$ samples prepared at different iron and phosphate concentrations (see text).

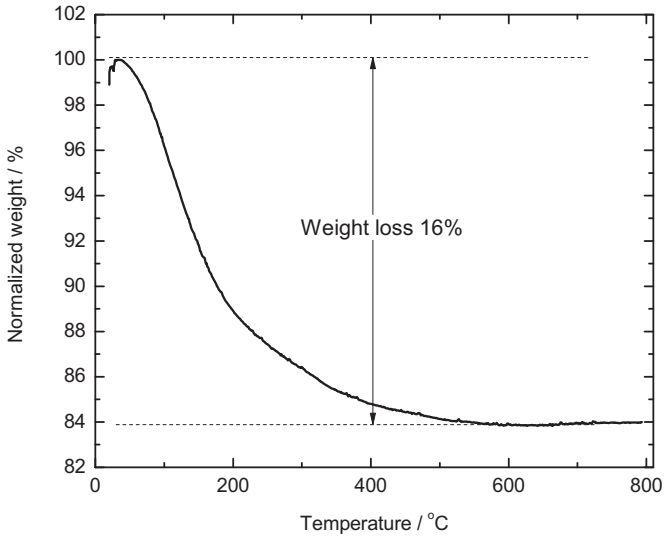

Fig. 3. Thermogravimetric measurement of amorphous, pristine $FePO_4 \cdot xH_2O$.

pristine, yellowish $FePO_4$ was fully amorphous, the characteristic diffraction pattern of $FePO_4$ could be obtained for all materials after thermal treatment. BET measurements revealed that the initial concentration within the precursor solvent plays a vital role with respect to the specific surface area (SSA) of the product. Assuming monodisperse, spherical particles, the respective particle size can be calculated from the SSA. It was found that the particle size increases from 12 to 18 nm in diameter with increasing precursor concentration while the SSA decreases from 218 to 126 $m^2\ g^{-1}$ (see Table 1). Annealing at 600 °C decreased the specific surface area significantly. The particle sizes derived from BET match well with those received from Rietveld refinement of the XRD pattern. As expected, the particles tend to grow during calcination but they still exhibit a high specific surface area and low particle sizes between 25 (30) and 72 (87) nm (numbers from BET and XRD, respectively).

As known from the work of Galoustov et al. iron phosphate typically contains some water molecules per unit cell. Therefore, thermogravimetry measurements were conducted to measure the amount of water of the pristine $FePO_4$ and to determine the temperature required for the formation of the anhydrous salt. Fig. 3 exhibits the thermogravimetry results for a temperature variation from room temperature to 800 °C in inert atmosphere at a heating rate of 10 °C min^{-1}. A weight loss of about 16 wt% was observed which corresponds to the presence of 1.7 mole water per mole $FePO_4$. The measurements show that a complete release of water requires a minimum temperature of about 600 °C.

Conductivity measurements (not shown) indicated that pristine $FePO_4 \cdot xH_2O$ produced from the 0.2 M precursor solution had the best electrical properties as this sample exhibited a three times larger conductivity than the samples synthesized from less concentrated precursor solution. Hence, this material was chosen for further processing to receive a nanostructured $LiFePO_4$/C composite material. The composite was prepared from $FePO_4 \cdot xH_2O$, Li_2CO_3 and glucose as described above. The added glucose acts as a reducing agent to reduce Fe^{3+} to Fe^{2+} during the formation of $LiFePO_4$ and we made use of the effect that carbon, formed from excess glucose, additionally inhibits particle growth [9,11,17,29]. This can be affirmed as can be seen from the results shown in Table 1. Excess of carbon is also known to enhance the electronic conductivity of $LiFePO_4$/C, thus providing improved electrochemical properties [1].

Table 1
Specific surface area and particle size of as-prepared and calcinated $FePO_4$ synthesized at various iron and phosphate concentrations.

Sample	As-prepared		Calcinated at 600 °C		
	Specific surface area [$m^2\ g^{-1}$]	Particle size D_{BET} [nm^{-1}]	Specific surface area [$m^2\ g^{-1}$]	Particle size D_{BET} [nm^{-1}]	Crystallite size [nm^{-1}]
FP0.0125	218	12	80	25	30
FP0.05	173	14	57	36	42
FP0.2	126	18	27	72	87
LFPC	24	69			70

Fig. 4 depicts the X-ray pattern of $LiFePO_4$/C synthesized at 600 °C. The pattern can be attributed to $LiFePO_4$ (olivine) and well indexed in the orthorhombic system (space group Pnma) with cell parameters of $a = 10.333$, $b = 6.012$, and $c = 4.697$ Å. The crystallite size obtained from Rietveld refinement showed very good agreement with D_{BET} (cf. Table 1). This result is consistent with the work of Yang et al. who synthesized $LiFePO_4$/C via a polymer–pyrolysis–reduction method [7]. According to the expectation that carbon species synthesized at 600 °C exist in an amorphous form, no diffraction peak of carbon was detected in the XRD pattern. The $LiFePO_4$/C had a deep black color while materials without excess of glucose were grey.

To validate the oxidation state of the iron atoms and to prove the existence of carbon in $LiFePO_4$/C, X-ray photoelectron spectroscopy (XPS) measurements were conducted and the result is presented in Fig. 5a. No other signals than those from lithium, iron, phosphorus, oxygen, and carbon were detected which confirmed that the prepared $LiFePO_4$/C is free from impurities that can be detected using this technique. The binding energy (BE) for Li1s, P2p, C1s and O1s were found to be 56, 134, 287, and 532 eV, respectively. The inset shows the enlarged spectrum at around 720 eV indicating Fe2p3/2 and Fe2p1/2 with binding energies of 725 and 712 eV, correspondingly. This result fully agrees with findings reported in literature [12,15,16]. These two peaks could be ascribed to the characteristic of Fe^{2+} in $LiFePO_4$. Thus, the XPS analysis further confirms that our $LiFePO_4$/C is of high purity.

The carbon content analyzed by CHNS elemental analysis revealed that the amount of carbon in $LiFePO_4$/C was 3.85 wt%. Even though carbon coating would offer better electronic conductivity, some groups report that at high amount of carbon would affect the electrochemical performance of $LiFePO_4$ [21,29] as the carbon layer

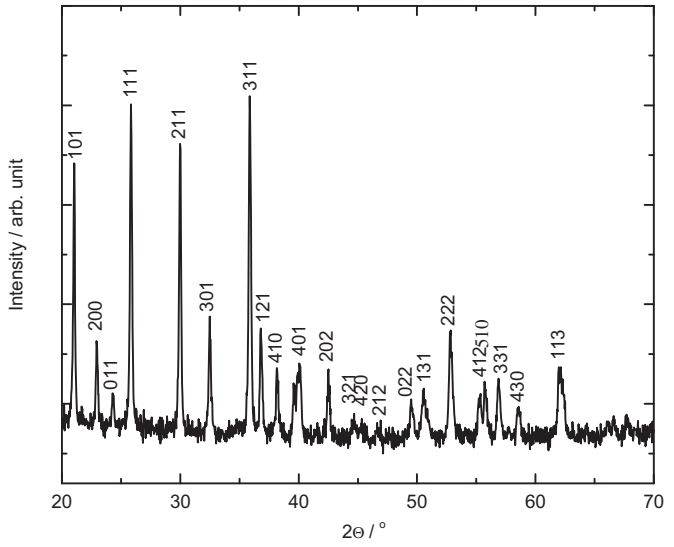

Fig. 4. XRD pattern of nano-$LiFePO_4$/C composite synthesized at 600 °C.

could hamper the formation of crystalline $LiFePO_4$ and reduce the tap density, which leads to lower energy density. Compared to values of about 1.05 g cm^2 reported in literature for composites with a carbon content of 3.5% [30], the tap density of our material is comparably high, and therefore a low volumetric energy density is not expected. The carbon phase within the $LiFePO_4$/C composite was further investigated using Raman spectroscopy. The spectrum showed two prominent peaks at the G-band (1584 cm^{-1}) and the D-band (1353 cm^{-1}, cf. Fig. 5b). The second-order signal was only visible as a small modulated bump (2400–3300 cm^{-1}) not shown here. These results clearly indicate the presence of carbon and show the characteristic features of the transition region from nano-crystalline to amorphous carbon as described by Ferrari and Robertson [31].

The morphology of the pristine amorphous, as well as the heat-treated crystalline $FePO_4$ and of $LiFePO_4$/C was studied using TEM as shown in Fig. 6a–c. Mostly, soft agglomerates of spherical particles were received directly after flame spray synthesis (Fig. 6a) which turned to fully necking, large and facetted aggregates after heat-treatment at 600 °C (Fig. 6b). Fig. 6c shows again mostly spherical particles of $LiFePO_4$ surrounded by a porous network of carbon. The image clearly supports the finding that the carbon phase prevents the $LiFePO_4$ from sintering together. It is also revealed that the carbon phase is homogenously distributed within the active material of $LiFePO_4$ thus enhancing the electronic conductivity and providing a better channel for the Li^+ ions diffusion during intercalation and de-intercalation.

The electrochemical performance of the nanosized $LiFePO_4$/C was investigated by cyclic voltammetry, constant-current charge/discharge measurements and electrochemical impedance spectroscopy. The influence of two different preparation steps during slurry production was investigated to identify the most suitable processing with respect to the electrochemical performance. Fig. 7 shows the voltammograms of the first cycle of nano-$LiFePO_4$/C electrodes processed from slurries prepared either by sonication or by using a turbo mixer. No significant differences were observed for the two samples. Two peaks around 3.5 V vs. Li/Li^+ for $LiFePO_4$/C were detected and a slight polarization was found in consistence to literature [4]. We examined a broad oxidation peak and a sharp reduction peak, associated with the oxidation of Fe(II) to Fe(III) and the corresponding reduction according to Eq. (1):

$$LiFe(II)PO_4 \rightarrow Li_{1-x}Fe(III_x/II_{1-x})PO_4 + xLi^+ + xe^- \quad (1)$$

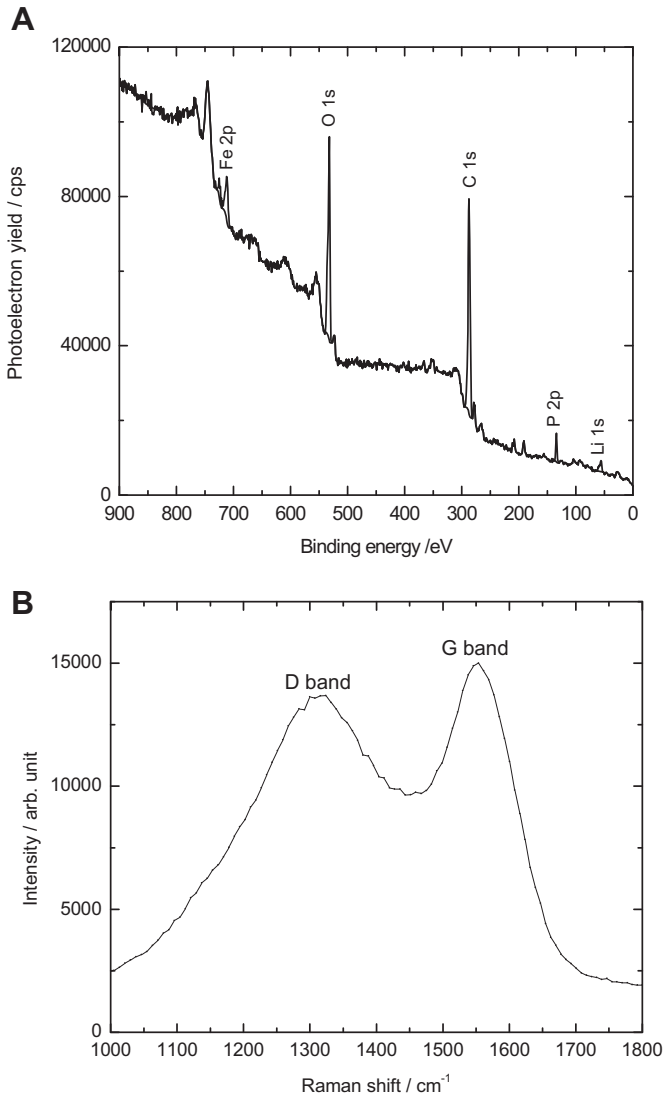

Fig. 5. (a) XPS spectrum of $LiFePO_4$/C. (b) Raman spectrum of $LiFePO_4$/C.

As can be seen from the inset in Fig. 7, the broad oxidation peak only appears during the first cycle while the subsequent cycling shows the typical symmetric behavior for charging and discharging. We attribute this to some initial restructuring taking place during the first cycle. The charges for the oxidation process received from integration of the respective signals were 161.7 mAh g^{-1} for the sonicated sample and 161.6 mAh g^{-1} for the turbo-mixed sample. Discharge capacities of 157.3 and 149.3 mAh g^{-1} were determined resulting in efficiencies of around 97 and 92%, respectively. These data imply that the electrochemical processes are reversible and that the broad shape of the oxidation peak cannot be explained by side reactions, e.g., decomposition of the electrolyte. Most likely, we attribute the unusual shape of this peak to diffusion limitations during the first cycle of the oxidation process. Additionally, differences regarding the shape of the reduction peak and the respective oxidation peak may be attributed to a modification of the electrode microstructure or an enhancement of wetting the nanosized $LiFePO_4$/C electrode during the first charging step. In addition, the distinction of the peak potentials referred to their maxima is 187 mV for the $LiFePO_4$/C electrode manufactured from turbo-mixed material and 199 mV for the sonicated sample. This finding is also in accordance with literature [4,8]. We assume that homogenization by

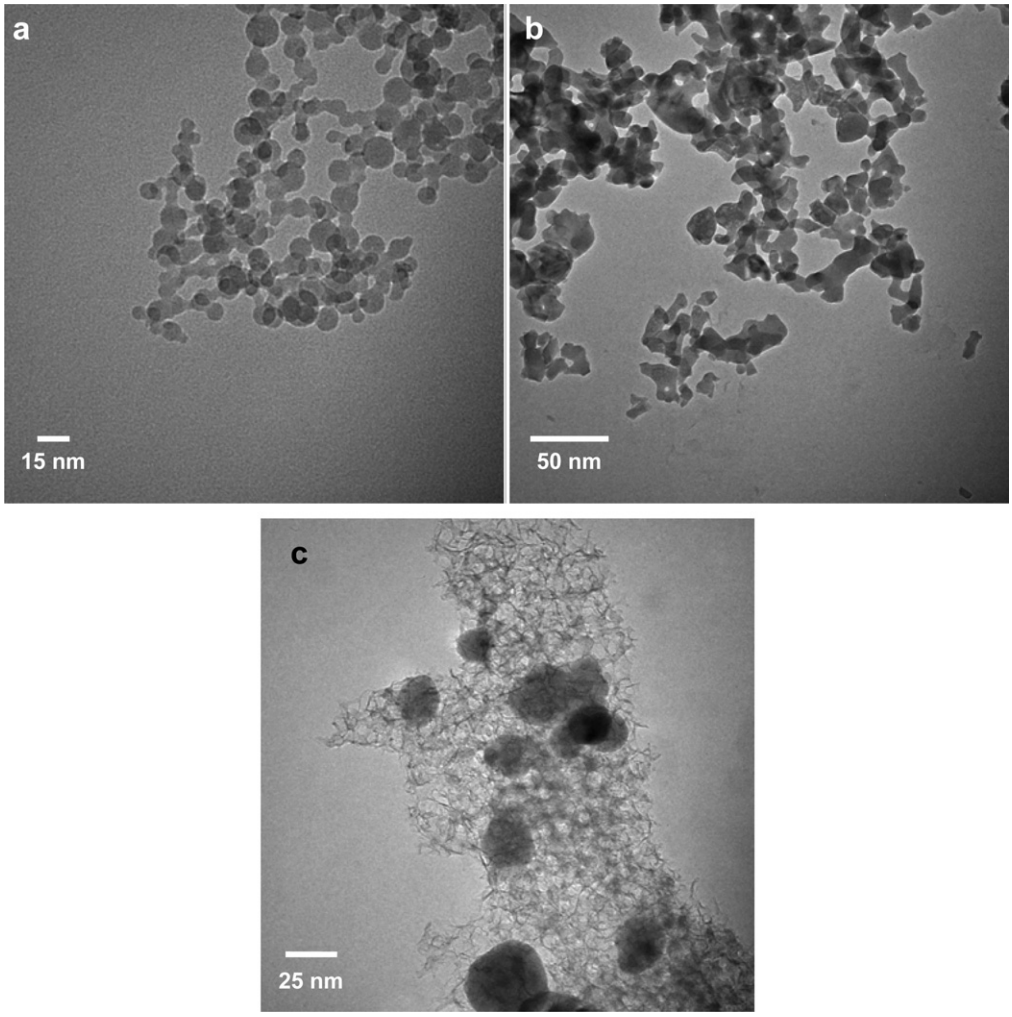

Fig. 6. TEM micrographs of $FePO_4$ from 0.2 M precursor solution (a) as-prepared (b) after annealing at 600 °C (c) $LiFePO_4$/C composite.

using a turbo mixer leads to better dispersion and increased electrical connection between active material, Super-P™, and binder.

Fig. 8 shows the discharge curves of nano-$LiFePO_4$/C samples recorded at 0.05 C. Flat potential plateaus at 3.4 V vs. Li/Li^+ were observed, which is typical for the single-phase transition of iron-phosphate to lithium ironphosphate (cf. Eq. (1)). Discharge capacities of 134 and 142 mAh g^{-1} were reached for $LiFePO_4$/C cathodes produced either by using a turbo mixer or sonication. These values are about 16 to 21% below the theoretical capacity limit of lithium iron phosphate. We attribute the reduced capacity to the intended limitation of the potential to 4.0 V we have chosen for our experiments. Usually, $LiFePO_4$/C cathodes are charged to a cut-off potential of 4.2 to 4.5 V to reach fully delithiated iron phosphate [3,24]. With respect to the large specific surface of our material compared to materials investigated in literature, we decided to limit the potential to 4.0 V vs. Li/Li^+ as unwanted side reactions with the electrolyte might occur at higher potential. However, by referring the observed capacities to the mass of the entire coating (including the electrochemical inactive materials), reversible capacities of 111 and 117 mAh g^{-1} were obtained, respectively, which is good compared to values of about 120 mAh g^{-1} reported in literature, whereat the charge cut-off voltages were set higher than 4.0 V [2,5,8].

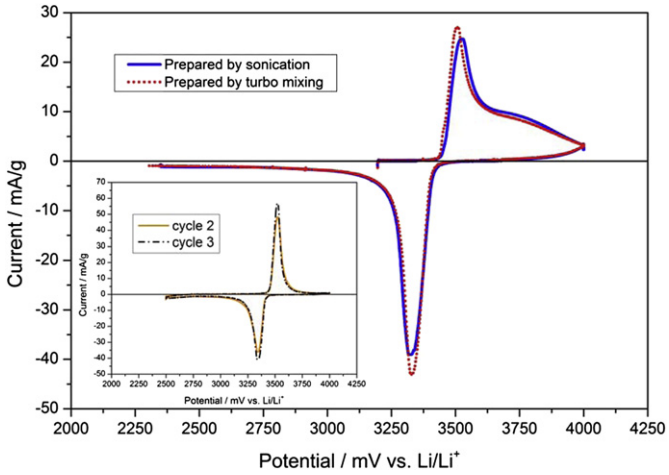

Fig. 7. Cyclovoltammogram of $LiFePO_4$/C composite electrodes measured at a scan rate of 0.01 mV/s. The inset shows the cyclovoltammograms of the 2nd and 3rd cycle indicating that the asymmetry observed for the first cycle can be attributed to an initial change in microstructure.

Fig. 9 illustrates the discharge capacities in dependence on the applied discharge C rate for the $LiFePO_4$/C electrodes processed via sonication und turbo mixing. As expected, in both cases the discharge capacities are reduced and the polarization is increased by increasing the C rate (Fig. 10). Due to the limited lithium-ion and electron diffusion rates in olivine structures, capacity losses result at high rates [22,32]. However, referred to the entire coating mass,

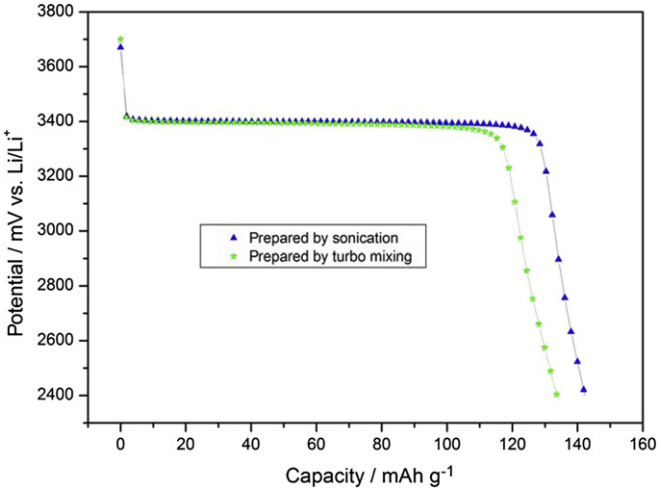

Fig. 8. Discharge curves of $LiFePO_4/C$ at a rate of 0.05 C.

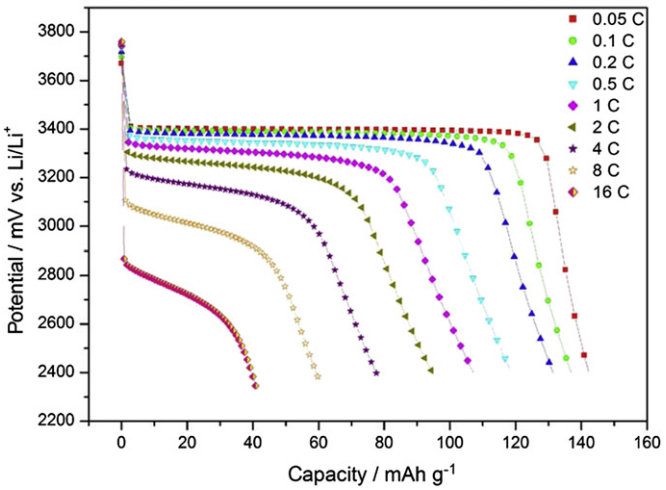

Fig. 10. Discharge curves of $LiFePO_4/C$ at various discharge rate for the sample prepared by sonication.

our nanosized lithium iron phosphate yields extraordinarily high reversible capacities even at very high rates of up to 40 mAh g^{-1} at 16 C. This is about 20% higher than the values reported by Waser et al. who used a very similar synthesis route but larger $LiFePO_4$ particles [26]. We attribute this very good performance of our material to the small particle size resulting in a large surface area and thus short diffusion paths. After high-rate exposure, the $LiFePO_4/C$ electrodes were cycled again at a C/10 rate and as can be seen from Fig. 9, the discharge capacities returned to at least their original value showing that the electrodes are very stable. Surprisingly, even improved capacities in comparison to the initial cycling at C/10 rate are observed indicating that the performance of our $LiFePO_4/C$ composite was enhanced during cycling. Despite the fact that the electrodes made from sonicated materials showed a higher polarization (see Fig. 7), slightly higher capacities were observed compared to electrodes prepared by turbo mixing.

A possible explanation for the increasing performance can be found from impedance measurements. Fig. 11 shows two Nyquist plots of the $LiFePO_4/C$ electrode prepared by sonication measured after the initial charge and discharge of the cells and after all cycling experiments. While the Ohmic resistance has slightly increased during cycling by approximately 2 Ω (the intersection point with the real axis has slightly shifted, see inset), the diameter of the semicircle – indicating the charge-transfer impedance of the system – has decreased by more than 80%. This can be explained by faster electrode kinetics and may be attributed to a change in the microstructure and/or the wetting of the $LiFePO_4/C$ composite within the electrode, see also Fig. 9.

4. Summary

Nanosized $FePO_4 \cdot xH_2O$ was synthesized using highly scalable and flexible flame spray pyrolysis whereas the particle size can be controlled by the concentration of the iron (III) precursor. High purity $LiFePO_4/C$ composite materials with particle sizes of 70 nm and 3.85 wt% of homogeneously distributed carbon were produced by a subsequent solid-state reaction providing material with a good discharge capacity of more than 140 mAh g^{-1} and elevated rate performance. Reversible capacities of 142 and 107 mAh g^{-1} at 0.1 C and 1 C were reached, respectively. In addition, the material was

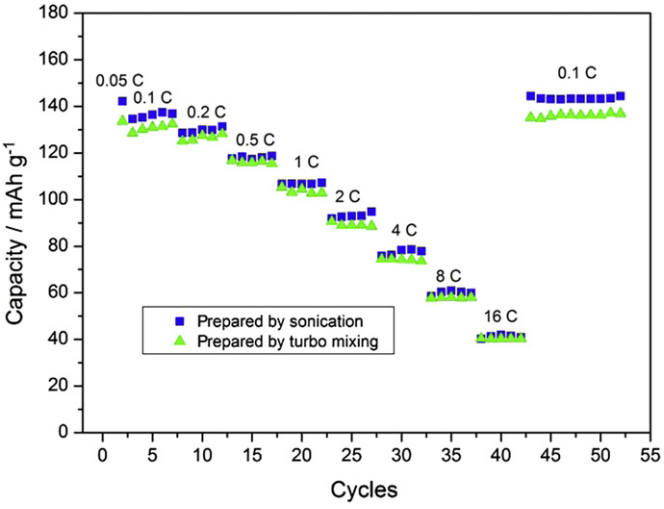

Fig. 9. Discharge capacities of $LiFePO_4/C$ pre-charged with a charge rate of 0.1 C (except for the first cycle which was set to 0.05 C). The cut-off voltages were adjusted to 2.4 and 4.0 V.

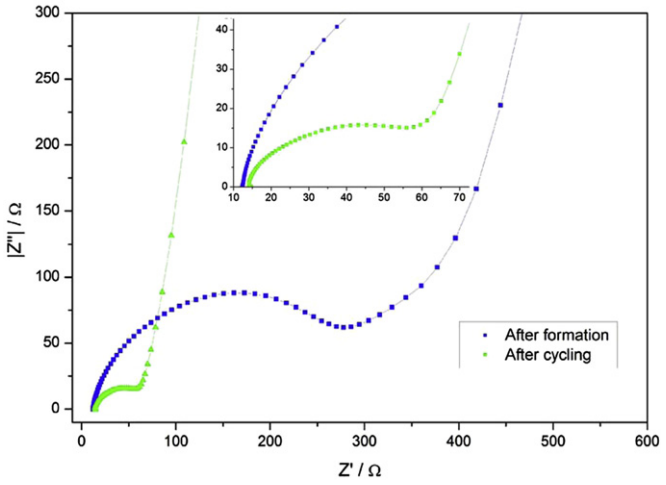

Fig. 11. Impedance spectra (Nyquist plots) of nano-$LiFePO_4/C$ electrode (prepared by sonication) which are recorded after the cell formation at 0.05 C and the CC experiments.

cycled up to 16 C and showed a good high-rate capability. In summary, the material shows excellent and improved capacity compared with the same material produced by various other sophisticated methods due to its reduced particle size. It has a great potential as cathode for high-capacity Li-ion batteries. Especially, the easy and scalable synthesis route makes our approach a highly promising way towards high capacity, safe, economic, and sustainable cathode materials.

Acknowledgments

Financial support by the European Union, and the Ministry of Innovation, Science and Research of the State of North Rhine-Westphalia in Germany (NanoEnergieTechnikZentrum, NETZ, Objective 2 Program: European Regional Development Fund, ERDF) is gratefully acknowledged. N.A. Hamid is thankful for financial support by the Ministry of Higher Education of Malaysia. The authors thank H. Grimm for help with TEM characterization, G. Prinz for help with Raman spectroscopy, and Hatice Karacuban for help with XPS spectroscopy.

References

[1] M.S. Whittingham, Chemical Reviews 104 (2004) 4271–4302.
[2] J. Liu, G. Yang, X. Zhang, J. Wang, R. Wang, Journal of Power Sources 197 (2012) 253–259.
[3] G. Wang, Y. Cheng, M. Yan, Z. Jiang, Journal of Solid State Electrochemistry 11 (2007) 457–462.
[4] A. Fedorková, R. Oriňáková, A. Oriňák, H.D. Wiemhöfer, D. Kaniansky, M. Winter, Journal of Solid State Electrochemistry 14 (2010) 2173–2178.
[5] N. Kalaiselvi, A. Manthiram, Journal of Power Sources 195 (2010) 2894–2899.
[6] H. Chen, W.Q. Gong, Y.L. Liu, J.H. Liu, Zhongguo Youse Jinshu Xuebao/Chinese Journal of Nonferrous Metals 20 (2010) 2206–2212.
[7] K. Yang, Z. Lin, X. Hu, Z. Deng, J. Suo, Electrochimica Acta 56 (2011) 2941–2946.
[8] W. Peng, L. Jiao, H. Gao, Z. Qi, Q. Wang, H. Du, Y. Si, Y. Wang, H. Yuan, Journal of Power Sources 196 (2011) 2841–2847.
[9] K.-F. Hsu, S.-Y. Tsay, B.-J. Hwang, Journal of Materials Chemistry 14 (2004) 2690–2695.
[10] X. Lou, Y. Zhang, Journal of Materials Chemistry 21 (2011) 4156–4160.
[11] Y. Huang, H. Ren, Z. Peng, Y. Zhou, Electrochimica Acta 55 (2009) 311–315.
[12] Y. Wang, B. Sun, J. Park, W.-S. Kim, H.-S. Kim, G. Wang, Journal of Alloys and Compounds 509 (2011) 1040–1044.
[13] K. Galoustov, M. Anthonisen, D.H. Ryan, D.D. MacNeil, Journal of Power Sources 196 (2011) 6893–6897.
[14] M.-S. Song, Y.-M. Kang, J.-H. Kim, H.-S. Kim, D.-Y. Kim, H.-S. Kwon, J.-Y. Lee, Journal of Power Sources 166 (2007) 260–265.
[15] H. Liu, D. Tang, Solid State Ionics 179 (2008) 1897–1901.
[16] L.N. Wang, Z.G. Zhang, K.L. Zhang, Journal of Power Sources 167 (2007) 200–205.
[17] X. Zhi, G. Liang, L. Wang, X. Ou, L. Gao, X. Jie, Journal of Alloys and Compounds 503 (2010) 370–374.
[18] L. Wang, G.C. Liang, X.Q. Ou, X.K. Zhi, J.P. Zhang, J.Y. Cui, Journal of Power Sources 189 (2009) 423–428.
[19] H. Liu, P. Zhang, G.C. Li, Q. Wu, Y.P. Wu, Journal of Solid State Electrochemistry 12 (2008) 1011–1015.
[20] X.-F. Guo, H. Zhan, Y.-H. Zhou, Solid State Ionics 180 (2009) 386–391.
[21] S.S. Zhang, J.L. Allen, K. Xu, T.R. Jow, Journal of Power Sources 147 (2005) 234–240.
[22] A.S. Andersson, J.O. Thomas, Journal of Power Sources 97–98 (2001) 498–502.
[23] W.L. Liu, J.P. Tu, Y.Q. Qiao, J.P. Zhou, S.J. Shi, X.L. Wang, C.D. Gu, Journal of Power Sources 196 (2011) 7728–7735.
[24] S.-H. Wu, K.-M. Hsiao, W.-R. Liu, Journal of Power Sources 146 (2005) 550–554.
[25] Y. Wang, J. Wang, J. Yang, Y. Nuli, Advanced Functional Materials 16 (2006) 2135–2140.
[26] O. Waser, R. Büchel, A. Hintennach, P. Novák, S.E. Pratsinis, Journal of Aerosol Science 42 (2011) 657–667.
[27] L. Mädler, H.K. Kammler, R. Mueller, S.E. Pratsinis, Journal of Aerosol Science 33 (2002) 369–389.
[28] S.M.L. Lutterotti, H.R. Wenk, in: ICUr: Newsletter of the CPD (1999), p. 14.
[29] A.F. Liu, Z.H. Hu, Z.B. Wen, L. Lei, J. An, Ionics 16 (2010) 311–316.
[30] Z.H. Chen, J.R. Dahn, Journal of the Electrochemical Society 149 (2002) A1184–A1189.
[31] A.C. Ferrari, J. Robertson, Physical Review B 61 (2000) 14095–14107.
[32] N. Ravet, Y. Chouinard, J.F. Magnan, S. Besner, M. Gauthier, M. Armand, Journal of Power Sources 97-98 (2001) 503–507.